Hindawi Publishing Corporation
International Journal of Antennas and Propagation
Volume 2015, Article ID 218751, 6 pages
http://dx.doi.org/10.1155/2015/218751

Research Article

Cylindrical Three-Dimensional Millimeter-Wave Imaging via Compressive Sensing

Guoqiang Zhao, Shiyong Li, Bailing Ren, Qingwei Qiu, and Houjun Sun

Beijing Key Laboratory of Millimeter Wave and Terahertz Technology, Beijing Institute of Technology, Beijing 100081, China

Correspondence should be addressed to Shiyong Li; lisy_98@bit.edu.cn

Received 31 December 2014; Revised 16 July 2015; Accepted 28 July 2015

Academic Editor: Ali Yapar

Millimeter-wave (MMW) imaging techniques have been used for the detection of concealed weapons and contraband carried by personnel. However, the future application of the new technology may be limited by its large number of antennas. In order to reduce the complexity of the hardware, a novel MMW imaging method based on compressive sensing (CS) is proposed in this paper. The MMW images can be reconstructed from the significantly undersampled backscattered data via the CS approach. Thus the number of antennas and the cost of system can be further reduced than those based on the traditional imaging methods that obey the Nyquist sampling theorem. The effectiveness of the proposed method is validated by numerical simulations as well as by real measured data of objects.

1. Introduction

Millimeter-wave (MMW) imaging techniques have been applied for the detection of concealed weapons and contraband carried by personnel at airports and other secure locations [1–5]. Millimeter waves can penetrate common clothing barriers to form an image of a person as well as any concealed items with different reflectivity or emissivity. Also, millimeter waves are nonionizing and, therefore, pose no known health hazard at moderate power levels, not like X-ray systems.

However, a large number of antennas and switches (maybe from hundreds to ten thousands) are needed to construct one- or two-dimensional (1D or 2D) array to obtain three-dimensional (3D) images, which increases the cost of the imaging system and then limits its wide application. In order to reduce the complexity and cost of the system, we propose a compressive sensing- (CS-) based method for 3D MMW imaging. The area of CS was initiated in 2006 by Candès et al. [6] and by Donoho [7].

CS has been widely explored in the domain of radar imaging [8–11], in which the image was usually converted into a vector. And the 1D optimization algorithm was used to recover the image. However, if we convert the 3D image into a vector, a huge sensing matrix will be introduced. Then the computational complexity will be largely increased. In this paper, we introduce an operator as the sensing matrix to represent the traditional imaging process based on wavenumber domain algorithm (WDA) [12]. Thus, large-scale matrix computations are avoided. The image resolution of the WDA is determined by signal bandwidth, signal frequency, and the length of synthetic aperture. And the resolution of the CS-based imaging algorithm is determined mainly by the signal-to-noise ratio and the matching degree of signal model to the requirements of CS, such as the restricted isometry property (RIP). The simulation and experiment results show that the CS-based method offers a much more accurate image than the traditional WDA just using a small subset of the full samples.

The rest of the paper is organized as follows. In Section 2, the CS imaging method based on the traditional WDA is introduced. The results demonstrating the efficiency and accuracy of the method are shown in Section 3. Section 4 summarizes the conclusions.

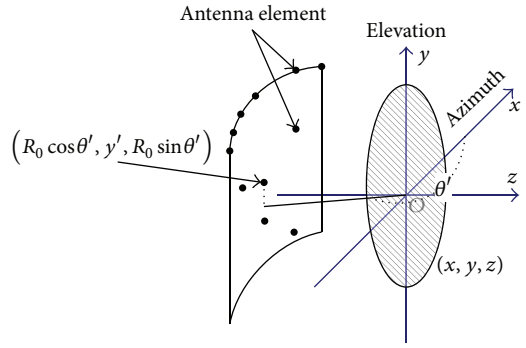

Figure 1: Cylindrical near-field 3D imaging configuration.

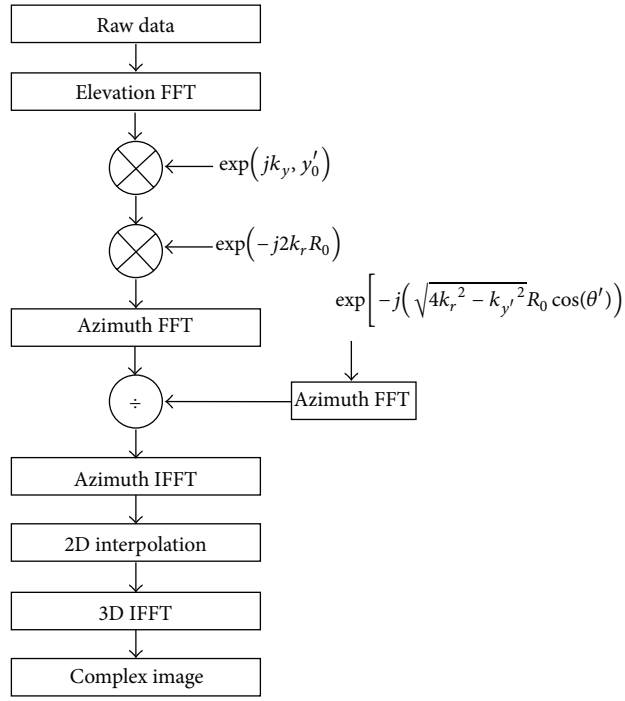

Figure 2: Scheme of the wavenumber domain algorithm.

2. CS-Based Method for 3D MMW Imaging

For the 3D imaging geometry is illustrated in Figure 1. An object formed by a distribution of independent scatterers of reflectivity $g(x, y, z)$ is located at the center of the imaging scene. The backscattered field $Y(k, \theta, y')$ after demodulation is given by

$$Y\left(k, \theta, y'\right) = \iiint_{x,y,z} g\left(x, y, z\right) \cdot \exp\left[-j2kR_{\theta,y'}\left(x, y, z\right)\right] \mathrm{d}x\, \mathrm{d}y\, \mathrm{d}z, \tag{1}$$

where $k = 2\pi f/c$ is the spatial frequency, c represents the light speed, $R_{\theta,y'}(x, y, z) = \sqrt{(R_0 \cos\theta - x)^2 + (R_0 \sin\theta - z)^2 + (y' - y)^2}$ is the distance from each antenna element at $(R_0 \cos\theta, y', R_0 \sin\theta)$ to each scattering center at (x, y, z), and R_0 is the radius of the cylindrical aperture, as shown in Figure 1.

The scheme of the traditional WDA [12] for near-field cylindrical 3D imaging is illustrated in Figure 2. We represent the imaging process as an operator. Then, the inverse process can be represented as the inversion of the operator. Thus the imaging process is given by

$$g\left(x, y, z\right) = G\left[Y\left(k, \theta, y'\right)\right], \tag{2}$$

where the operator G denotes the imaging process as shown in Figure 2; that is,

$$G = \mathrm{IFFT}_{3\mathrm{D}}\left\{\mathrm{IN}_{2\mathrm{D}}\left\{\mathrm{IFFT}_{k_\theta}\left\{\mathrm{FFT}_{\theta}\left[\mathrm{FFT}_{y'}\left(\cdot\right)\right] \cdot \mathrm{FFT}_{\theta}\left\{\exp\left[jk_{xz}R_0 \cos\left(\theta\right)\right]\right\}\right\}\right\}, \tag{3}$$

where $\mathrm{IN}_{2\mathrm{D}}(\cdot)$ represents 2D interpolation.

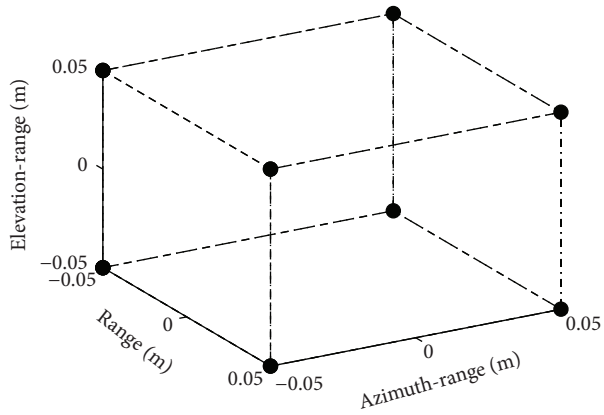

Figure 3: Target model.

Then $Y(k, \theta, y')$ can be expressed as the inversion of (2) as follows:

$$Y\left(k, \theta, y'\right) = G^{-1}\left[g\left(x, y, z\right)\right], \tag{4}$$

where G^{-1} denotes the inverse process of (3).

Due to the sparsity of the image scene $g(x, y, z)$, only a small subset of scattered data $Y(k, \theta, y')$ is enough to be used to reconstruct the image exactly by solving the optimization problem [13]:

$$\begin{aligned} \min_{g} \quad & \left\|\psi g\left(x, y, z\right)\right\|_0 \\ \text{s.t.} \quad & Y\left(k, \theta, y'\right) = G^{-1}\left[g\left(x, y, z\right)\right], \end{aligned} \tag{5}$$

where $\|\cdot\|_0$ is simply the number of nonzero components of ψg, and ψ represents a sparse transform, making ψg a sparse vector.

However, solving (5) is an NP-hard problem and thus practically not feasible. Instead, its convex relaxation is usually considered as

$$\begin{aligned} \min \Big\{ & \left\|Y\left(k, \theta, y'\right) - G^{-1}\left[g\left(x, y, z\right)\right]\right\|_2^2 \\ & + \lambda \left\|\psi g\left(x, y, z\right)\right\|_1 \Big\}, \end{aligned} \tag{6}$$

where $\|\cdot\|_1$ and $\|\cdot\|_2$ denote the ℓ_1 norm and ℓ_2 norm, respectively. In this paper, we use the total-variation (TV) as a sparse transform. The parameter λ is used to balance the twin objectives of minimizing both error and sparsity.

The operators G and G^{-1} correspond to the Fourier matrices if we express the signal model directly. Thus, G and G^{-1} satisfy the RIP required by CS, and both (5) and (6) have the same unique solution [6]. There are many state-of-the-art optimization algorithms designed to solve the convex optimization problem of (6) [14–17]. Here we use a nonlinear conjugate gradient (CG) descent algorithm described in [18]. The computational complexities of $G^{-1}[g(x, y, z)]$ and $G[Y(k, \theta, y')]$ both are an order of (NMP)·$\log_2$(NMP)+NMP· K, N, M and P are the sizes of the scattered data, K being the interpolator length. And the computational complexity of the key part of the CG algorithm during an iteration is an order of (NMP)$\log_2$(NMP) [18].

Table 1: Simulation parameters for full set of samples.

Parameters	Values
Center frequency (GHz)	91
Bandwidth (GHz)	10
Sampling interval along azimuth-range direction (m)	0.004
Number of samples along azimuth-range direction	64
Sampling interval along elevation-range direction (m)	0.004
Number of samples along elevation-range direction	64

3. Results

The aforementioned algorithm is tested with numerical simulations and experimental data. The simulation parameters are shown in Table 1. Figure 3 shows the target model with 8 point-like scatterers with equal radar cross section. The 3D imaging result (isosurface of −13 dB relative to the maximum value) of WDA using the full sampling data and the result of the proposed CS-based method using only 25% of the full data are shown in Figures 4(a) and 4(b), respectively. Clearly, even with a small subset of the full data, the CS-based method can provide a more accurate imaging result with higher resolution than WDA.

The experiments on real measured data are performed. A stepped-frequency W-band radar with two circular polarized horn antennas is used for the measurement, which is shown in Figure 5. Three screws and a card are measured, respectively, as shown in Figure 6. The diameter of the cross section of the screw is about 1 cm.

The corresponding MMW imaging results of WDA using the full measured data are shown in Figures 7(a) and 8(a), respectively. And the results of the CS-based method using only 25% of the full data are demonstrated in Figures 7(b) and 8(b), respectively. Due to the fact that the card is a distributed target, the imaging result in Figure 8(b) is not so good as the point-like target in Figure 7(b). However, the main characteristics remained; for example, the chip inside the card can be easily seen in Figure 8(b).

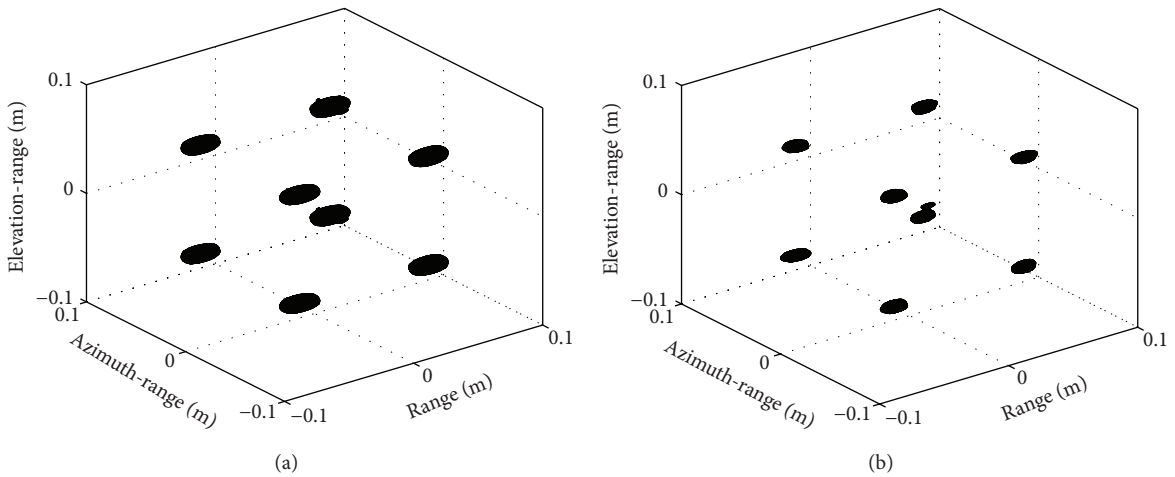

Figure 4: 3D MMW images of the target model: (a) the result of WDA using the full data and (b) the result of the CS-based method using only 25% of the full data.

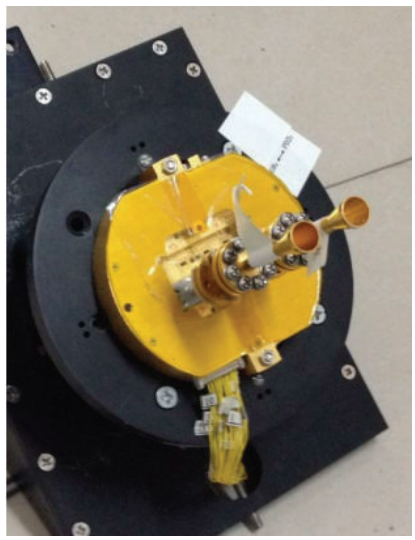

Figure 5: W-band measurement radar.

Figure 6: Photo of three screws and a card.

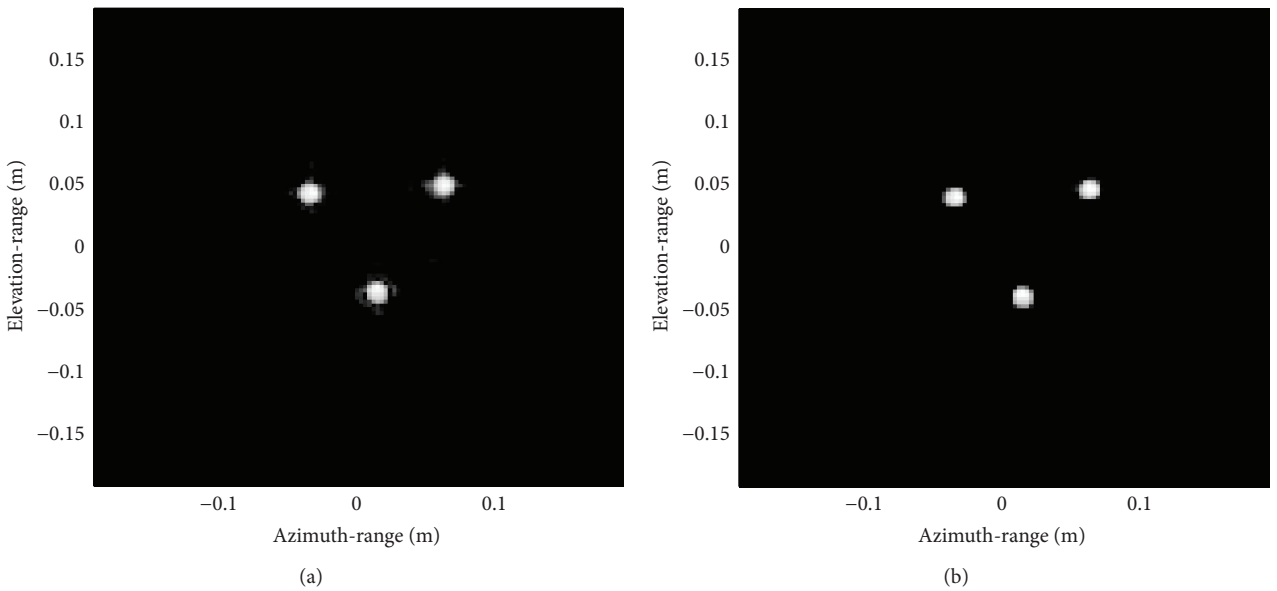

Figure 7: MMW images of the screws: (a) the result of WDA using the full data and (b) the result of the CS-based method using only 25% of the full data.

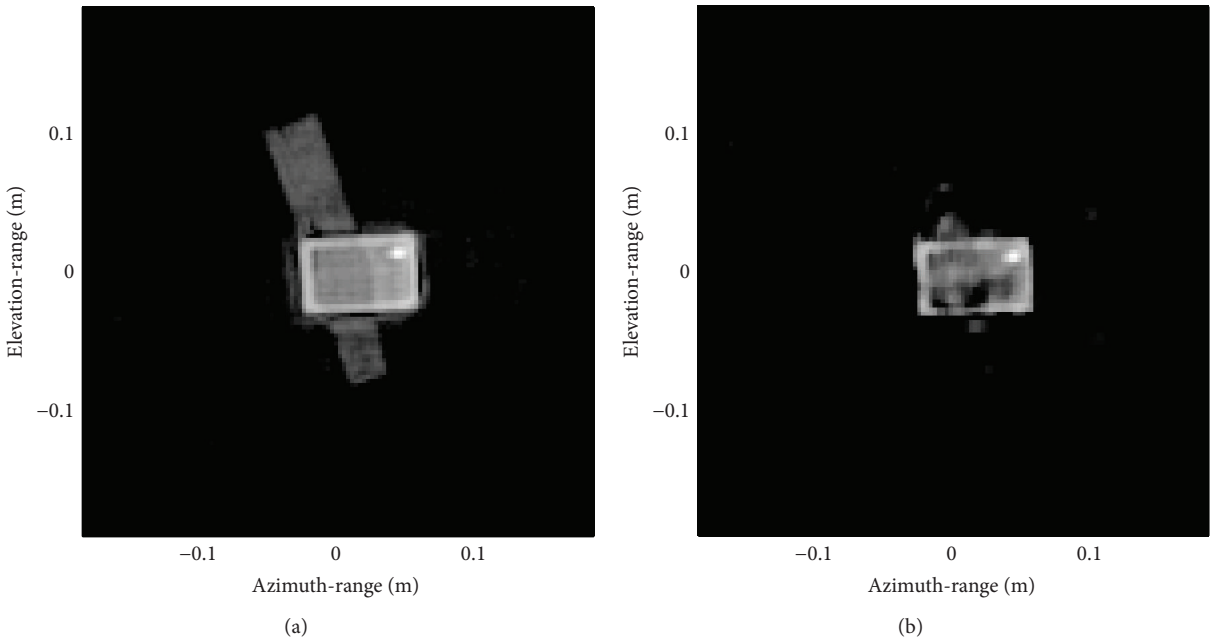

Figure 8: MMW images of the card: (a) the result of WDA using the full data and (b) the result of the CS-based method using only 25% of the full data.

4. Conclusion

A CS-based method has been proposed for cylindrical near-field 3D MMW imaging. The imaging process and its inversion are represented by an operator and its inversion, respectively, to avoid large-scale matrix computation. Thus the CS approach can be applied to the cylindrical 3D imaging by using the operator as the sensing matrix. Simulation and experiment results show that the CS-based method can offer highly accurate and reliable results, even using only a small subset of the full samples compared with the traditional wavenumber domain algorithm.

Conflict of Interests

The authors declare that there is no conflict of interests regarding the publication of this paper.

References

[1] D. M. Sheen, D. L. McMakin, and T. E. Hall, "Three-dimensional millimeter-wave imaging for concealed weapon detection," *IEEE Transactions on Microwave Theory and Techniques*, vol. 49, no. 9, pp. 1581–1592, 2001.

[2] R. Appleby and R. N. Anderton, "Millimeter-wave and submillimeter-wave imaging for security and surveillance," *Proceedings of the IEEE*, vol. 95, no. 8, pp. 1683–1690, 2007.

[3] D. M. Sheen, D. McMakin, and T. E. Hall, "Near-field three-dimensional radar imaging techniques and applications," *Applied Optics*, vol. 49, no. 19, pp. E83–E93, 2010.

[4] S. S. Ahmed, A. Genghammer, A. Schiessl, and L.-P. Schmidt, "Fully electronic E-band personnel imager of 2 m2 aperture based on a multistatic architecture," *IEEE Transactions on Microwave Theory and Techniques*, vol. 61, no. 1, pp. 651–657, 2013.

[5] D. M. Sheen and T. E. Hall, "Reconstruction techniques for sparse multistatic linear array microwave imaging," in *Passive and Active Millimeter-Wave Imaging XVII*, vol. 9078 of *Proceedings of SPIE*, p. 12, June 2014.

[6] E. J. Candès, J. Romberg, and T. Tao, "Robust uncertainty principles: exact signal reconstruction from highly incomplete frequency information," *IEEE Transactions on Information Theory*, vol. 52, no. 2, pp. 489–509, 2006.

[7] D. L. Donoho, "Compressed sensing," *IEEE Transactions on Information Theory*, vol. 52, no. 4, pp. 1289–1306, 2006.

[8] R. G. Baraniuk and P. Steeghs, "Compressive radar imaging," in *Proceedings of the IEEE Radar Conference*, pp. 128–133, April 2007.

[9] L. C. Potter, E. Ertin, J. T. Parker, and M. Çetin, "Sparsity and compressed sensing in radar imaging," *Proceedings of the IEEE*, vol. 98, no. 6, pp. 1006–1020, 2010.

[10] X. Zhang, P. Huang, and X. Li, "2D SAR imaging scheme based on compressive sensing," *Electronics Letters*, vol. 50, no. 2, pp. 114–116, 2014.

[11] W. J. Zhang and A. Hoorfar, "A generalized approach for SAR and MIMO radar imaging of building interior targets with compressive sensing," *IEEE Antennas and Wireless Propagation Letters*, vol. 14, pp. 1052–1055, 2015.

[12] D. M. Sheen, D. L. McMakin, T. E. Hall, and R. H. Severtsen, "Real-time wideband cylindrical holographic surveillance system," US Patent 5 859 609, 1999.

[13] S. Sun, G. Zhu, and T. Jin, "Novel methods to accelerate CS radar imaging by NUFFT," *IEEE Transactions on Geoscience and Remote Sensing*, vol. 53, no. 1, pp. 557–566, 2015.

[14] Y. Nesterov, *Introductory Lectures on Convex Optimization. A Basic Course*, Kluwer Academic Publishers, Boston, Mass, USA, 2004.

[15] J. A. Tropp and A. C. Gilbert, "Signal recovery from random measurements via orthogonal matching pursuit," *IEEE Transactions on Information Theory*, vol. 53, no. 12, pp. 4655–4666, 2007.

[16] M. A. T. Figueiredo, R. D. Nowak, and S. J. Wright, "Gradient projection for sparse reconstruction: application to compressed sensing and other inverse problems," *IEEE Journal on Selected Topics in Signal Processing*, vol. 1, no. 4, pp. 586–597, 2007.

[17] A. Beck and M. Teboulle, "A fast iterative shrinkage-thresholding algorithm for linear inverse problems," *SIAM Journal on Imaging Sciences*, vol. 2, no. 1, pp. 183–202, 2009.

[18] M. Lustig, D. Donoho, and J. M. Pauly, "Sparse MRI: the application of compressed sensing for rapid MR imaging," *Magnetic Resonance in Medicine*, vol. 58, no. 6, pp. 1182–1195, 2007.